Chemical Physics Letters 808 (2022) 140118

Contents lists available at ScienceDirect

Chemical Physics Letters

journal homepage: www.elsevier.com/locate/cplett

Transition Metal−N/Graphene for advanced Lithium–Sulfur Batteries: A first principles study

Yang Zhang [a,b], Song Lu [a], Kingsley Ugochukwu [b], Fengliu Lou [b,*], Zhixin Yu [a,*]

[a] Department of Energy and Petroleum Engineering, University of Stavanger, 4036 Stavanger, Norway
[b] Beyonder AS, Stokkamyrveien 30, 4313, Sandnes, Norway

ARTICLE INFO

Keywords:
Anchoring materials
Electrocatalytic effect
Li−S battery
TM–N–C
First principles study

ABSTRACT

Developing highly efficient anchoring materials with strong adsorption to lithium polysulfides to suppress 'shuttling effect' is crucial to address the short cycling life issue of lithium sulfur batteries. Herein, we systematically investigated transition metal, nitrogen co-doped graphene as host materials for sulfur cathode via first-principles study. The computation results reveal that TM_2–N—C materials have higher adsorption energy to lithium polysulfides than TM–N—C materials. Fe_2–N—C is one of the most promising anchoring materials, where robust Fe–S and N–Li bonds ensure the stable adsorption of all LiPSs.

1. Introduction

Currently, lithium-ion batteries (LiBs) play a dominant role in energy storage devices because of their advantages of high energy density, long cycling life and good reliability [1,2]. The development of new technology for energy storage is highly desired to meet the requirements of emerging applications such as electrical vehicle (EVs) [3,4]. Lithium-sulfur batteries (LiSBs) are considered as one of the next generation energy storage devices because their advantage in energy density is over the state-of-the-art commercial LiBs [5–8]. In addition, the abundance of sulfur, environmental friendliness and the low cost make LiSBs more attractive for industrial application [9–11]. However, some issues, including the limited utilization of sulfur, the large volume variation during cycling, and the shuttling effect need to be addressed for the commercialization of LiSBs [11–15].

Considerable efforts have been dedicated to tackle the aforementioned challenges. Inspiringly, Ji et al. developed a highly-ordered porous carbon material as sulfur host to immobilize the high order lithium polysulfides (LiPSs) (Li_2S_n, n = 4, 6, 8) [16]. Since then, using porous carbon as anchoring materials for sulfur has become one of the most popular strategies to physically enclose LiPSs [17,18]. Graphene nanosheet has been regarded as promising sulfur host in LiSBs for its excellent electrical/thermal conductivity and great flexibility [18–20]. However, the physical interaction between nonpolar graphene and polar LiPSs is too weak to hinder the shuttling effect. To overcome this obstacle, heteroatoms with stronger electronegativity were introduced to carbon materials to promote their capability to block LiPSs. Several heteroatom doped carbon materials revealed enhanced electrochemical performance when employed as sulfur hosts [21–27]. Particularly, N atom is the most extensively utilized dopant for carbon based sulfur anchoring materials for LiSBs [22,24,26,27]. For instance, Qiu et al. reported that pyrrolic and pyridinic *N*-doped graphene show stronger combination with LiPSs through covalent bonds than pristine graphene [22]. Three-dimensional (3D) structure can alleviate volume variation during charge/discharge cycling, which is favorable for sulfur entrapment. Chao et al. synthesized porous 3D nitrogen-doped graphene to wrap sulfur [28]. The loading of sulfur reached to 87.6 wt%, and the LiSBs exhibited exceptional good rate capability and stability.

Benefitting from their special electrocatalytic properties, incorporating TM into sulfur host materials in LiSBs possesses a lot of advantages [29–33]. TM and heteroatoms, especially nitrogen atom co-doped graphene based materials (TM–N—C) as multifunctional sulfur anchoring materials for LiSBs have been broadly explored both theoretically and experimentally with promising prospect [29,30,32–34]. Most of the studied TM–N—C materials are single transition metal atom doping. For example, Zeng et al. showed that Fe, N co-doped graphene has strong interaction with Li_2S_n, which prevents the dissolution and diffusion of Li_2S_n (n = 4, 6, 8). The adsorption strength can be further adjusted by varying the concentration of doping atoms [30]. Besides increasing the adsorption of Li_2S_n (n = 4, 6, 8), the conversion of soluble

* Corresponding authors at: Department of Energy and Petroleum Engineering, University of Stavanger, 4036 Stavanger, Norway (Zhixin Yu). Beyonder AS, Stokkamyrveien 30, 4313, Sandnes, Norway (Fengliu Lou).
E-mail addresses: fengliu@beyonder.no (F. Lou), zhixin.yu@uis.no (Z. Yu).

https://doi.org/10.1016/j.cplett.2022.140118
Received 22 June 2022; Received in revised form 13 September 2022; Accepted 5 October 2022
Available online 10 October 2022

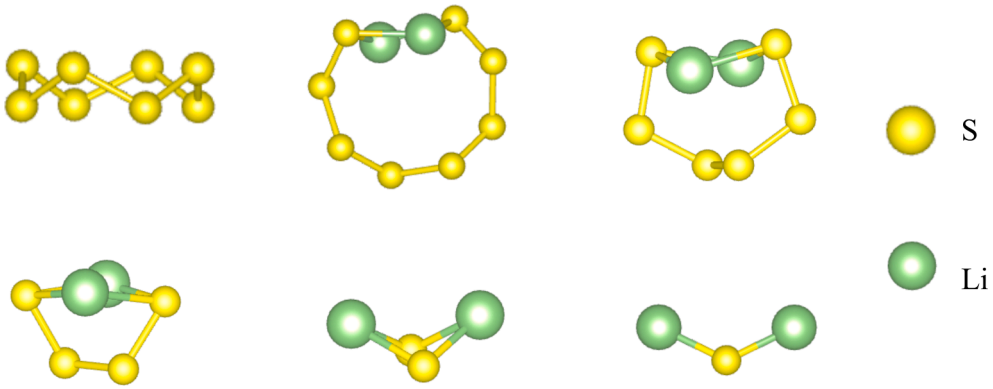

Fig. 1. The optimized structures of isolated cyclo–S_8 and Li_2S_n (n = 8, 6, 4, 2, and 1).

high order LiPSs to insoluble Li_2S_n (n = 1, 2) is another effective approach to ease shuttling effect [31,35–37]. For instance, He et al. revealed that Cr doped C_6N_2 monolayer could effectively accelerate the conversion of LiPSs and anchor lithium polysulfide during discharging while decrease the decomposition energy barrier of Li_2S during charging [38]. In addition to simulation, the advantage of TM–N—C materials in LiSBs has also been verified experimentally. Kim et al. reported a local coordination structure modification of Fe–N_4 moieties via morphological engineering of graphene support. Fe–N—C catalysts showed decent performance at high C-rates with promising cycling stability, resulting from the synergistic combination of atomic-level modified Fe–N_4 active sites and graphene support [39].

Combining TM catalysts with 3D porous structure as sulfur host materials can demonstrate even better electrochemical performance in LiSBs. A 3D hierarchical porous graphene embedded with evenly distributed α-Fe_2O_3 nano-particles can chemically promote the transformation of soluble LiPSs to insoluble low order insoluble LiPSs species [37]. Furthermore, rapid catalytic oxidation of Li_2S/Li_2S_2 back to S is also a useful mean to facilitate the utilization of sulfur [14,29,32–34]. For example, He et al. reported that TM@C_2N monolayers can decrease the decomposition energy of Li_2S, and Co@C_2N shows the largest adsorption energies of LiPSs and the lowest decomposition energy of Li_2S [14]. Zhang et al. demonstrated that Fe–N_4 and Cr–N_4 co-doped graphene shows strong adsorption of all Li_2S_n species and reduced decomposition energy of Li_2S/Li_2S_2, contributing to improved electrochemical performance of LiSBs [32]. Recently, a pair of iron atoms coordinated to nitrogen in the C_2N pores has been synthesized with significant enhancement in rate capability and cycling stability. The decomposition energy of Li_2S decreased greatly in C_2N/Fe system, thus enhancing the utilization of sulfur and resulting in good cycling stability with a deterioration rate of 0.013 % per cycle [33]. Therefore, TM, nitrogen co-doped graphene with either single metal atom or metal atoms pair doping as sulfur host materials are very promising in LiSBs, and more systematic research is desirable.

Herein, three earth-abundant metals (Fe, Co and Ni) were anchored into nitrogen doped graphene as single and diatomic doped materials Fe–N—C, Co–N—C, Ni–N—C, Fe_2–N—C, Fe/Co–N—C, Fe/Ni–N—C, Co_2–N—C, Co/Ni–N—C, Ni_2–N—C, which were investigated as potential sulfur host materials by performing first principles computations. To evaluate the performance of TM–N—C as sulfur host materials, their adsorption strength of Li_2S_n (n = 1, 2, 4, 6, 8) species, electrical conductivity and the catalytic oxidation capabilities of Li_2S were studied. Our results revealed that all diatomic systems show stronger interaction with Li_2S_n species compared with single metal atom doped materials. Particularly for Fe_2–N—C, it not only shows strong adsorption of LiPSs species, but also demonstrates the lowest decomposition energy of Li_2S. The electrical conductivity of diatomic systems is also well-maintained, demonstrating great potential as sulfur host for LiSBs.

Table 1
The average bond length (d) of isolated Li_2S_n species and cyclo–S_8, with unit Å.

LiPSs	Li_2S	Li_2S_2	Li_2S_4	Li_2S_6	Li_2S_8	cyclo–S_8
d_{S-Li}	2.09	2.22	2.39	2.82	4.27	–
d_{S-S}	–	2.19	2.11	2.04	2.09	2.06

2. Computational method

The Vienna ab initio simulation package code (VASP) with Project-Augmented Wave (PAW) pseudopotential was used to carry out spin polarized calculations [40,41]. The Perdew-Burke-Ernzerhof (PBE) approach within Generalized Gradient Approximation (GGA) were implemented to treat the exchange–correlation function of the interacting electrons [42,43]. A plane wave cutoff of 500 eV was applied for the kinetic energy calculation. 4 × 4 × 1 and 8 × 8 × 1 Monkhorst-Pack k-point mesh was conducted for structural relaxation and electronic calculations [44]. A 20 Å vacuum space along the z direction was inserted to eliminate the interactions of the adjacent periodic images. All structural optimizations were performed under the convergence criterion that energy and force were set to 1.0×10^{-5} and 0.01 eV/Å, respectively. The adsorption energies E_{ad} of LiPSs (*cyclo*-S_8) molecule and TM–N—C were defined by the following formula:

$$E_{ad} = E_{sub} + E_{mole} - E_{tot} \quad (1)$$

where E_{tot} is the total energy of TM–N—C with adsorbed LiPSs or cyclo–S_8, E_{sub} is the energy of TM–N—C, while E_{mole} is the energy of isolated LiPSs or cyclo–S_8 molecule. According to this definition, a positive value indicates an energetically favorable reaction.

The decomposition energy (ΔE) can be calculated by the equation below [14]:

$$\Delta E = E_{intact} - E_{decomposition} \quad (2)$$

where E_{intact} and $E_{decomposition}$ represent the total energy of Li_2S and Li + LiS adsorbed TM–N—C, respectively.

3. Results and discussion

3.1. Structures of Li_2S_n species and TM–N—C

In the discharge process of LiSBs, the Li_2S_n (n = 1, 2, 4, 6, 8) species are formed by incorporating additional Li cations, and the final product is Li_2S. The optimized structures of Li_2S_n (n = 1, 2, 4, 6, 8) and the most stable allotrope of S atoms, orthorhombic α–S_8 species are shown in Fig. 1. All LiPSs species are in a 3D shape, which is well in line with previous studies [29,31], indicating the reliability of our calculations. The bond length of Li–S (d_{Li-S}) and S—S (d_{S-S}) are listed in Table 1 for both isolated LiPSs and cyclo–S_8. The average d_{Li-S} of low-order Li_2S_n (n

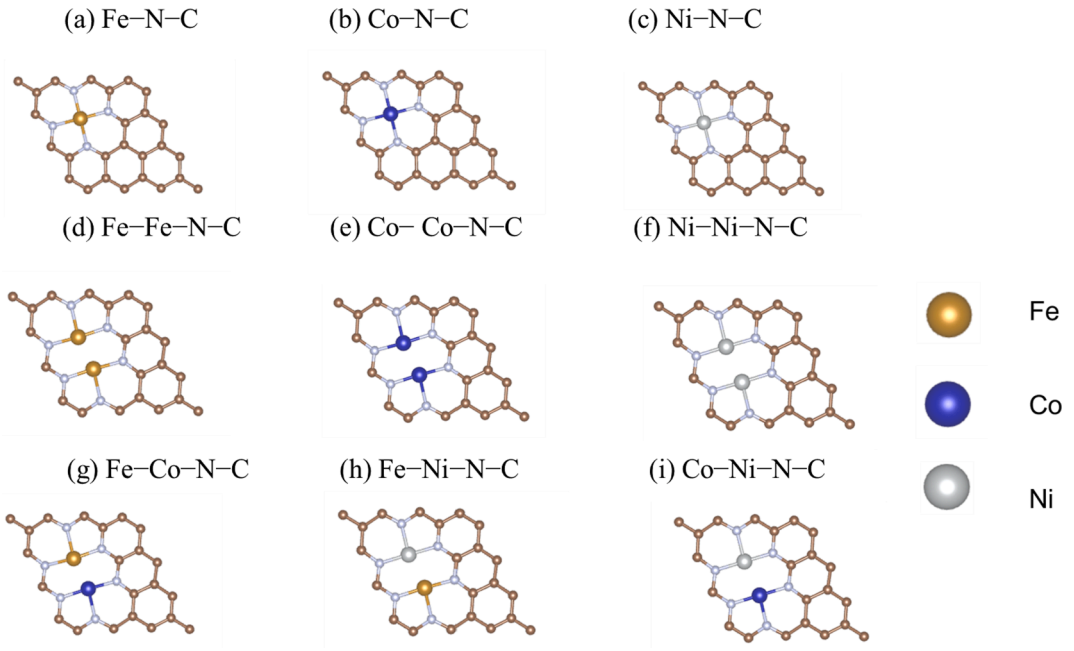

Fig. 2. The optimized structures of TM–N—C, TM = (a) Fe, (b) Co, (c) Ni, (d) Fe–Fe, (e) Co–Co, (f) Ni–Ni, (g) Fe–Co, (h) Fe–Ni, (i) Co–Ni.

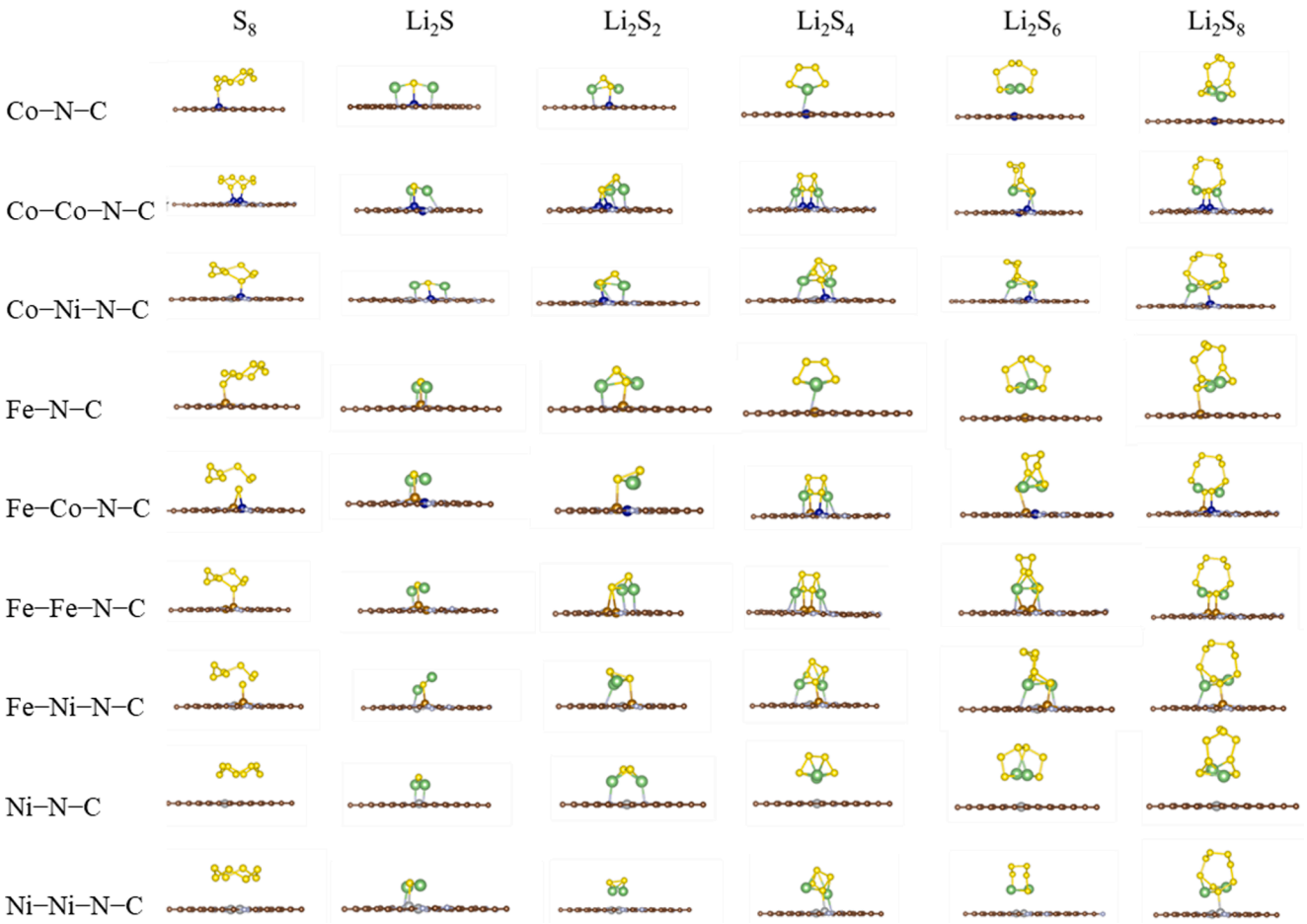

Fig. 3. The optimized structures of (a) S_8, (b) Li_2S, (c) Li_2S_2, (d) Li_2S_4, (e) Li_2S_6, (f) Li_2S_8 adsorbed on TM–N—C.

= 1, 2) species (2.16 Å) is significantly shorter than that of high-order Li_2S_n (n = 4, 6, 8) species (3.16 Å), while d_{S-S} slightly decrease with the increase of S atoms (n = 1, 2, 4, 6). However, the d_{S-S} in Li_2S_8 is slightly larger than that of Li_2S_6 but shorter than that in Li_2S_4. Generally, a longer bond implies a weaker chemical binding for the same type of bond. Therefore, the high-order Li_2S_n species will be more easily

Table 2
The adsorption energies E_{ad} (eV) and the average bond length d (Å) of Li_2S_n species and cyclo–S_8 after adsorption on Fe–N—C.

LiPSs	Li_2S	Li_2S_2	Li_2S_4	Li_2S_6	Li_2S_8	cyclo–S_8
E_{ad}	1.94	1.63	0.68	0.63	1.02	1.03
d_{Fe-S}	2.29	2.25	3.47	3.51	2.67	2.07
d_{Li-S}	2.18	2.34	2.41	2.37	2.42	–
d_{S-S}	–	2.14	2.07	2.07	2.08	2.15

Table 3
The adsorption energies E_{ad} (eV) and the average bond length d (Å) of Li_2S_n species and cyclo–S_8 after adsorption on Fe_2–N—C.

LiPSs	Li_2S	Li_2S_2	Li_2S_4	Li_2S_6	Li_2S_8	cyclo–S_8
E*ad*	2.22	1.93	1.54	1.42	1.43	1.25
d_{Fe-S}	2.28	2.78	2.43	2.43	2.43	2.21
d_{Li-S}	2.17	2.48	2.44	2.44	2.46	–
d_{S-S}	–	2.14	2.10	2.11	2.11	2.15

Table 4
The adsorption energies E_{ad} (eV) and the average bond length d (Å) of Li_2S_n species and cyclo–S_8 after adsorption on Fe–Ni–N—C.

LiPSs	Li_2S	Li_2S_2	Li_2S_4	Li_2S_6	Li_2S_8	cyclo–S_8
E_{ad}	1.93	1.82	1.54	1.51	1.52	1.11
d_{Fe-S}	2.40	2.62	2.29	2.26	2.25	2.03
d_{Ni-S}	–	4.31	3.53	3.45	3.36	4.04
d_{Li-S}	2.14	2.38	2.40	2.38	2.54	–
d_{S-S}	–	2.13	2.06	2.10	2.04	2.07

dissolved into lithium cations and polysulfide anions than low-order Li_2S_n species in the electrolyte of LiSBs.

Single TM atoms coordinating with four N atoms and TM atoms pair binding to six N atoms have been demonstrated with good stability [29,33], thus we only considered two defects by removing one and two C atoms from the graphene structure and then anchoring the TM atoms into vacancy in a 2 × 2 × 1 supercell. As shown in Fig. 2, all atoms of the TM–N—C structure are in the same plane after structure optimization. For the TM–N—C strucutre, the central TM atom is surrounded by four equivalent TM–N bonds. The bond lengths of TM–N (d_{TM-N}) are 1.89,1.87 and 1.87 Å for Fe, Co and Ni–N—C (Table S1), respectively, which are consistent with previous studies [29,30]. For the TM_2–N—C, two metal atoms are anchored into the vacancy and each metal atom is surrounded by three TM–N bonds. It can be found that there is no obvious difference in bond length of the same TM–N among different structures. For instance, d_{Fe-N} of Fe–N—C (1.89 Å) is quite close to d_{Fe-N} of Fe/Co–N—C (1.91 Å), Fe_2–N—C (1.91 Å) and Fe/Ni–N—C (1.91 Å), which demonstrates that dual-metal atoms anchored graphene can also have excellent stability as the single metal atom doped graphene.

3.2. Adsorption of Li_2S_n and cyclo–S_8 species on TM–N—C

Generally, the pristine graphene is not an ideal sulfur anchoring material for LiPSs because the van der Waals interactions between graphene and LiPSs are not strong enough to stabilize the adsorbed LiPSs species [19,45]. TM atoms are considered as the only active sites to adsorb LiPSs since TM atoms can improve the interaction between the graphene support and LiPSs species. After geometry optimization, the most stable configurations of LiPSs species and cyclo–S_8 adsorbed on TM–N—C are presented in Fig. 3. The key parameters such as average d_{Li-S}, d_{S-S}, d_{Li-N}, and d_{TM-S} of Fe–N—C, Fe_2–N—C and Fe/Ni–N—C are summarized in Table 2, Table 3 and Table 4. For example, the cyclo–S_8 adsorbed on the surface of Fe–N—C has the shortest distance (2.07 Å) between S and Fe atom (Table 2), which is close to the covalent ionic radius, indicating the formation of Fe–S bond. Meanwhile, some extent

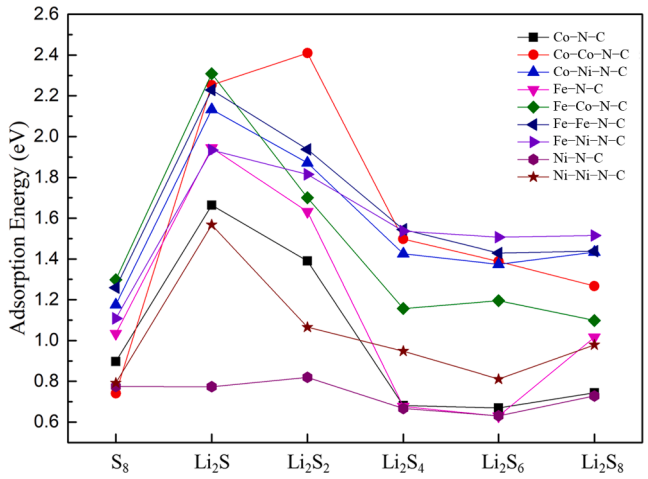

Fig. 4. The adsorption energy profile of cyclo–S_8 and Li_2S_n (n = 1, 2, 4, 6, 8) species after adsorption on TM–N—C (TM = Fe, Co, Ni) surface.

of structural distortion of adsorbed cyclo–S_8 can be evidenced via d_{S-S} stretching from 2.06 Å of the isolated cyclo–S_8 to 2.15 Å (Tables 1 and 2). These results indicate that LiPSs species could be activated by TM atom. For single TM–N—C, one sulfur atom binds with the metal atom, while one or two lithium atoms bind with nitrogen atoms in low order Li_2S_n, forming a chemical ring configuration. However, these binding ring structures become distorted after incorporating TM atoms pair, especially in Fe/Ni–N—C, which can be attributed to the different electronegativity of the heterogenous atom pair. For high order Li_2S_n (n = 4, 6, 8), single TM–N—C shows similar adsorption structures to these isolated species. However, these species can obviously be activated by Fe_2–N—C and Fe/Ni–N—C, as evidenced by the distorted configuration of the species. In addition, TM–N—C as support can well maintain their structures, and the Li_2S_n and S_8 species adjust themselves for the most stable adsorption, implying the metal embedded graphene with excellent stability.

To further investigate the ability of TM–N—C to alleviate the shuttling effect, adsorption energies of all Li_2S_n and S_8 species on TM–N—C systems were calculated (Fig. 4 and Table S2). For instance, the adsorption energy of S_8 molecule on dual atoms system such as Fe/Co–N—C, Fe_2–N—C and Co/Ni–N—C are 1.29, 1.25, 1.17 eV. The adsorption energy of S_8 molecule on single atom system including Fe–N—C, Co–N—C, Ni–N—C are only 1.03, 0.89 and 0.77 eV, respectively, which is much less than dual TM–N—C. All adsorption energy of TM–N—C increases significantly after incorporating the second TM atoms. Besides, robust chemical rings with large adsorption energies make the adsorption configuration more stable, resulting in a high affinity for low order Li_2S_n (n = 1, 2). Notably, the adsorption energies of high-order Li_2S_n species on Fe_2–N—C and Fe/Ni–N—C are clearly larger than that of others, which means that the high-order Li_2S_n species prefer to adsorb on Fe_2–N—C and Fe/Ni–N—C. For example, the adsorption energy of Fe/Ni–N—C to Li_2S_6 and Li_2S_8 is 1.51, 1.52 eV, which is the largest among nine different TM–N—C. The large adsorption energy to LiPSs indicates that Fe_2–N—C and Fe/Ni–N—C, as the best candidates among the considered anchoring materials, can most effectively adsorb Li_2S_n (n = 4, 6, 8) molecules to suppress the shuttling effect. Particularly, after Li_2S and Li_2S_2 adsorption on Fe_2–N—C, the Li–S bond length prolongs more significantly compared with the isolated state (Tables 1 and 3). The average d_{Li-S} after absorption increase from 2.09 Å to 2.17 Å for Li_2S, and 2.22 Å to 2.48 Å for Li_2S_2, respectively. The extension of the Li–S bond makes it easier to break, which is beneficial for the detachment of lithium ion. In addition to Fe-based TM–N—C, Co_2–N—C is also promising for shuttling effect alleviation with 2.25, 2.40, 1.49 eV adsorption energy to Li_2S, Li_2S_2, Li_2S_4, respectively. However, the adsorption energy of Co_2–N—C to Li_2S_6 and Li_2S_8 is not as large as Fe-

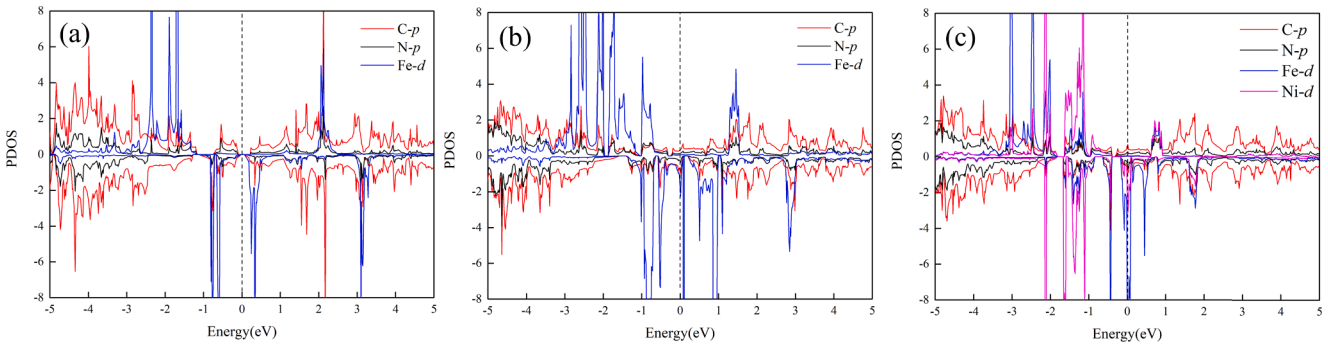

Fig. 5. The projected density of states (PDOS) of TM–N—C (TM = Fe (a), Fe–Fe (b), and Fe–Ni (c)).

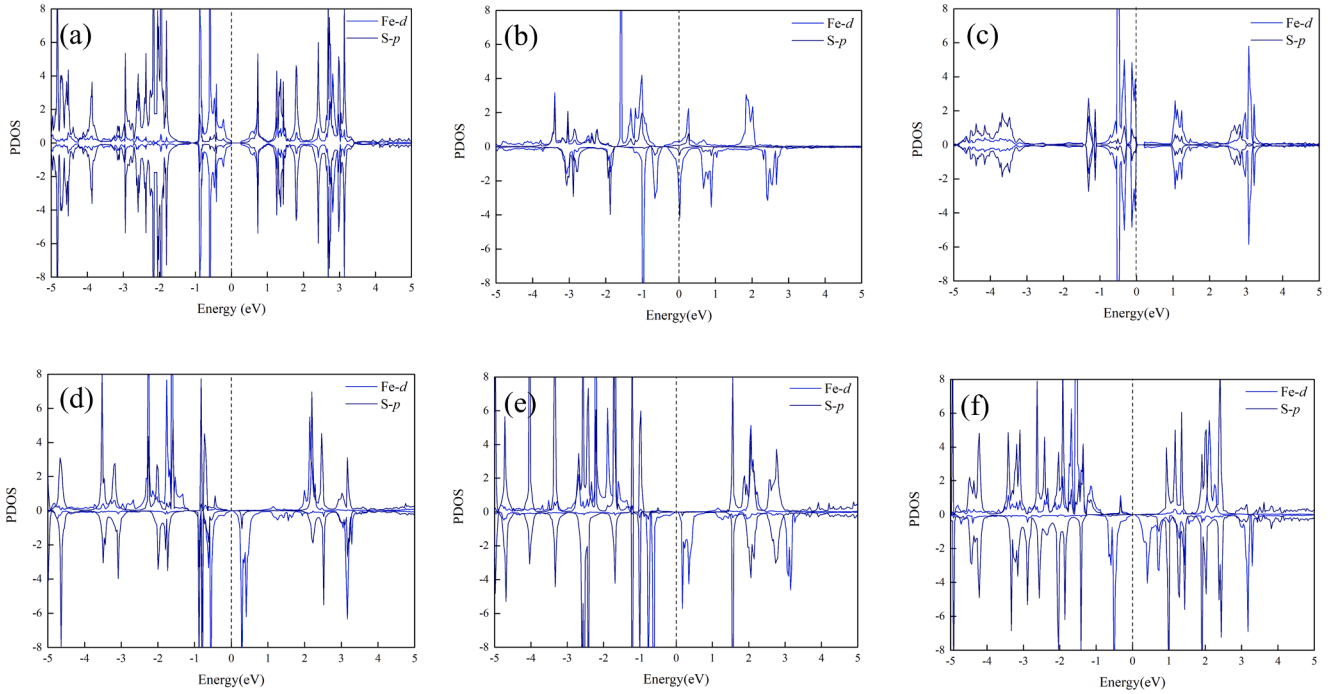

Fig. 6. The projected density of states (PDOS) of Fe–N—C with LiPSs adsorbed, LiPSs = (a)S_8, (b)Li_2S, (c)Li_2S_2, (d)Li_2S_4, (e)Li_2S_6, (f)Li_2S_8.

based TM–N—C. Subsequently, we focus on Fe_2–N—C for further detailed studies on the mechanism of Li_2S decomposition.

3.3. *Electronic properties of Fe based TM–N—C*

The electronic properties of graphene could be tuned by introducing external atoms [18]. Considering good adsorption of Fe_2–N—C and Fe/Ni–N—C to LiPSs, their electronic structures were studied by the projected density of states (PDOS). To compare, electronic structures of single atom Fe–N—C was also studied as illustrated in Fig. 5. Obviously, the *d*-state of metal atoms and *p* states of C/N atoms have remarkable interaction in both conduction and valence band. The PDOSs of Fe–N—C exhibit asymmetry in spin up and down for each element, indicating the magnetic properties. Furthermore, the magnetism mainly originates from its relatively localized *d*-orbital electrons of TM atoms both in conduction and valence band. Notably, there are more electron states near and even across the Fermi energy in Fe_2–N—C and Fe/Ni–N—C than Fe–N—C (Fig. 5), showcasing the activity of 3*d*-electrons. The introduced TM atoms contributed to the more localized electrons both in valence and conduction band, promoting electrons mobility. Therefore, the electrical conductivity of Fe–N—C is noticeably improved, which is beneficial for the performance of LiSBs. *d* band centre has been widely used to indicate the adsorption strength of intermediates on catalysts [46,47]. The *d* band centres of Fe–N—C, Fe_2–N—C and Fe/Ni–N—C are −1.24, −1.00 and −1.51 eV. Obviously, Fe_2–N—C show the highest energy that is close to Fermi level, indicating stable adsorption. It also suggests that Fe_2–N—C can be an effective anchoring material for Li_2S_n species.

The electronic structures including PDOS and charge density difference can be also investigated to estimate the adsorption of Li_2S_n species on Fe based TM–N—C. It can be found that the Fe-*d* and S-*p* states of Li_2S_n and S_8 species demonstrate obvious interactions both in conduction band and valence band (Figs. 6-8). Noticeably, Fe_2–N—C with dual Fe atoms exhibits more overlap of electron states. These results suggest that incorporating dual Fe atoms into graphene could obviously improve the interaction between Li_2S_n species and host materials. Considering Fe_2–N—C is one of the most effective anchoring materials for Li_2S_n species and the low price compared to other metal, the charge density difference of Li_2S_n and S_8 species adsorbed on Fe_2–N—C was further studied. The charge density difference indicates that there are many electrons locating on the Fe–S (Fig. 9). Fe atoms act as electron donor while S atoms are electron acceptor. Therefore, the Li_2S_n and S_8 species are activated by the Fe_2–N—C.

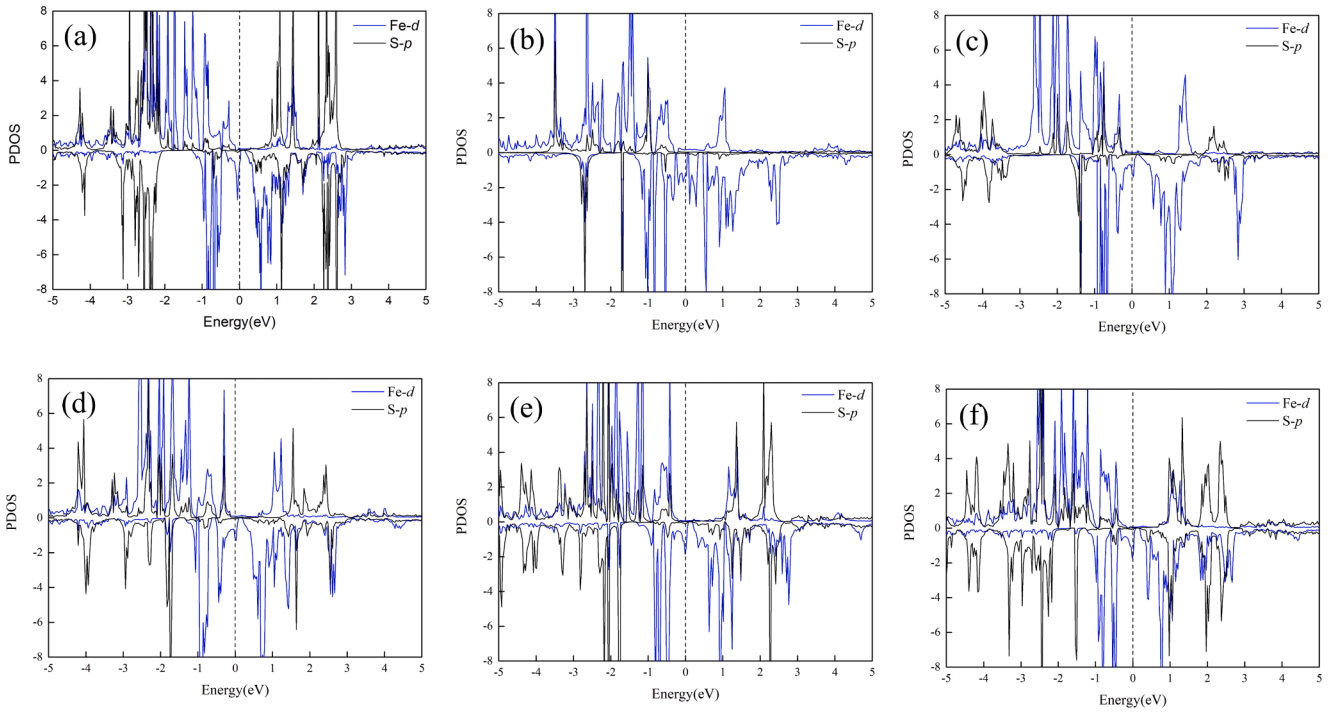

Fig. 7. The projected density of states (PDOS) of Fe_2–N—C with LiPSs adsorbed, LiPSs = (a)S_8, (b)Li_2S, (c)Li_2S_2, (d)Li_2S_4, (e)Li_2S_6, (f)Li_2S_8.

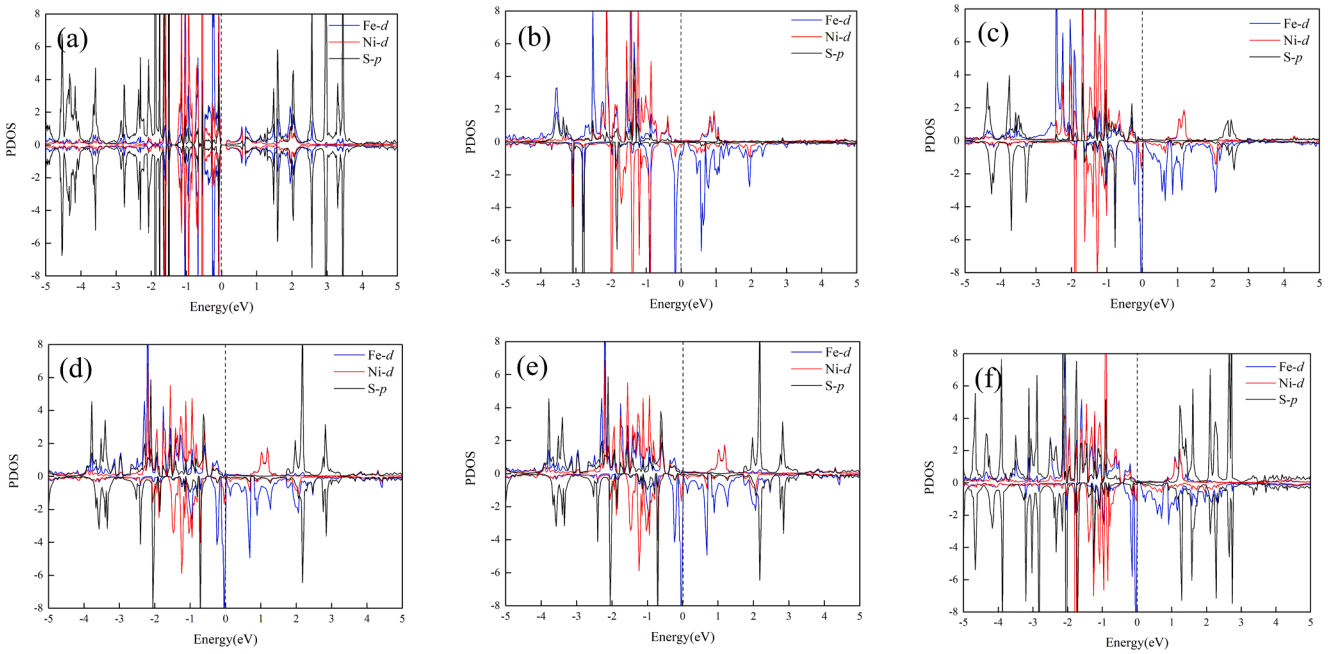

Fig. 8. The projected density of states (PDOS) of Fe–Ni–N—C with LiPSs adsorbed, LiPSs = (a)S_8, (b)Li_2S, (c)Li_2S_2, (d)Li_2S_4, (e)Li_2S_6, (f)Li_2S_8.

3.4. Electrocatalytic performance of TM–N—C for Li_2S_n species

The decomposition of the deep discharge products Li_2S on anchoring materials is a critical factor for energy density, sufur utilization, and cycling performance of LiSBs. An Li_2S molecule breaking into a LiS cluster and a single Li ion ($Li_2S \rightarrow LiS + Li^+ + e$) was considered as the decomposition process. The decomposition energy (ΔE) on nine different TM–N—C were shown in Fig. 10. It is obvious that Fe_2–N—C has the smallest decomposition energy of 0.63 eV, which is also much lower than that of pristine graphene (2.06 eV). Low decomposition energy of Li_2S is expected to increase the utilization of active materials. In brief, Fe_2–N—C can be a promising support for catalyzing low order LiPSs in the charging process of LiSBs.

Therefore, the anchoring material Fe_2–N—C can not only effectively adsorb the high order LiPSs to suppress the shuttling effect, but also drastically improve the electronic conductivity and decrease the decomposition energy of Li_2S. It could consequently achieve multiple targets and address several challenges of LiSBs.

4. Conclusions

Based on first-principles study, we systematically investigated the

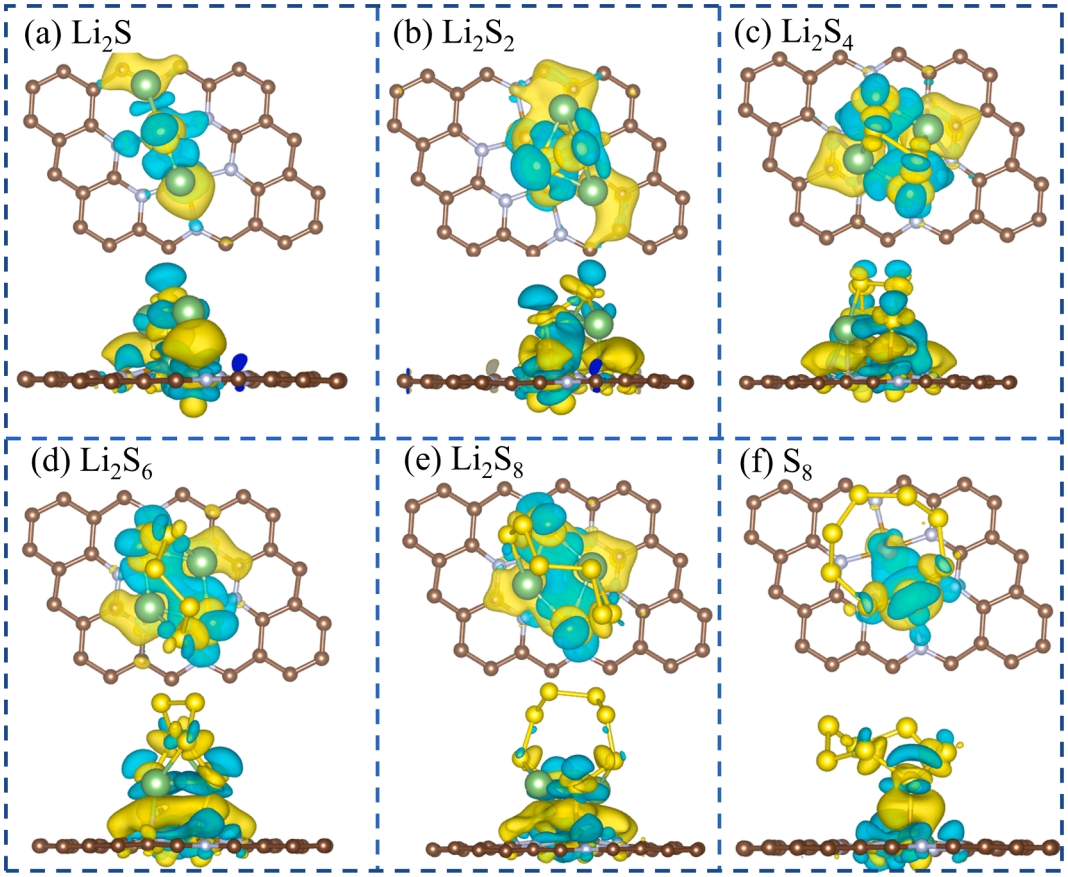

Fig. 9. The differential charge density distribution for LiPSs species adsorbed on Fe_2–N—C. The electron accumulation (depletion) region is shown in yellow (cyan). The value of the isosurface is set to 0.01 e Bohr–3. (For interpretation of the references to colour in this figure legend, the reader is referred to the web version of this article.)

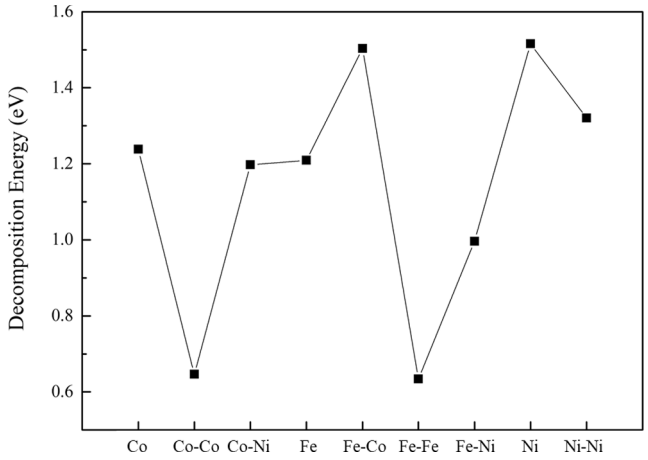

Fig. 10. The decomposition energy of Li_2S on TM–N—C (TM = Fe, Co, Ni).

TM–N—C (TM = Fe, Co, and Ni) as multi-functional anchoring materials to hinder the shuttling effect of LiPSs in LiSBs. Our calculations reveal that introducing second TM atom (TM_2–N—C) could not only dramatically improve the adsorption strength of Li_2S_n species and cyclo–S_8, but also enhance the electronic conductivity, which is mainly attributed to the strong chemical bonds of TM–S and N–Li. Fe_2–N—C is the best anchoring material among the nine investigated TM–N—C, because it has good adsorption to all LiPSs species, improved electric conductivity and the lowest decomposition energy for Li_2S. Our findings enrich the fundamental understanding of the mechanism of TM–N—C as multifunctional sulfur anchoring materials on micro-level and shed light on the design of high performance LiSBs.

CRediT authorship contribution statement

Yang Zhang: Conceptualization, Data curation, Investigation, Methodology, Visualization, Writing - original draft, Writing - review & editing. **Song Lu:** Data curation, Methodology, Visualization, Investigation, Writing - review & editing. **Kingsley Ugochukwu:** . **Fengliu Lou:** Supervision, Formal analysis, Funding acquisition, Resources, Writing - review & editing. **Zhixin Yu:** Supervision, Validation, Writing - review & editing.

Declaration of Competing Interest

The authors declare that they have no known competing financial interests or personal relationships that could have appeared to influence the work reported in this paper.

Data availability

Data will be made available on request.

Acknowledgement

The authors would like to thank the Norwegian Research Council and Beyonder AS for the financial support of this project under project No.310353.

Appendix A. Supplementary data

Supplementary data to this article can be found online at https://doi.org/10.1016/j.cplett.2022.140118.

References

[1] B. Dunn, H. Kamath, J.M. Tarascon, Electrical Energy Storage for the Grid: A Battery of Choices, Science 334 (2011) 928–935.
[2] M. Armand, J.-M. Tarascon, Building better batteries. *nature* 451 (2008) 652–657.
[3] M. Sathiya, G. Rousse, K. Ramesha, C. Laisa, H. Vezin, M.T. Sougrati, M.-L. Doublet, D. Foix, D. Gonbeau, W. Walker, Reversible anionic redox chemistry in high-capacity layered-oxide electrodes, Nat. Mater. 12 (2013) 827–835.
[4] G. Tan, F. Wu, Y. Yuan, R. Chen, T. Zhao, Y. Yao, J. Qian, J. Liu, Y. Ye, R. Shahbazian-Yassar, Freestanding three-dimensional core–shell nanoarrays for lithium-ion battery anodes, Nat. Commun. 7 (2016) 1–10.
[5] H.J. Peng, J.Q. Huang, X.B. Cheng, Q. Zhang, Lithium-Sulfur Batteries: Review on High-Loading and High-Energy Lithium–Sulfur Batteries (Adv. Energy Mater. 24/2017), Adv. Energy Mater., 2017, 7, 1770141.
[6] A. Manthiram, S. Chung, Zu C, Progress and Prospects. Advanced Materials, Lithium-Sulfur Batteries, 2015, p. 27.
[7] L. Lin, F. Pei, J. Peng, A. Fu, J. Cui, X. Fang, N. Zheng, Fiber network composed of interconnected yolk-shell carbon nanospheres for high-performance lithium-sulfur batteries, Nano Energy 54 (2018) 50–58.
[8] X. Ji, L.F. Nazar, Advances in Li–S batteries, J. Mater. Chem. 20 (2010) 9821–9826.
[9] J. Song, M.J. Choo, H. Noh, J.K. Park, H.T. Kim, Perfluorinated Ionomer-Enveloped Sulfur Cathodes for Lithium-Sulfur Batteries, ChemSusChem 7 (2014) 3341–3346.
[10] K. Zhu, C. Wang, Z. Chi, F. Ke, Y. Yang, A. Wang, W. Wang, L. Miao, How far away are lithium-sulfur batteries from commercialization? Front. Energy Res. 123 (2019).
[11] R. Fang, S. Zhao, Z. Sun, D.W. Wang, H.M. Cheng, F. Li, More reliable lithium-sulfur batteries: status, solutions and prospects, Adv. Mater. 29 (2017) 1606823.
[12] Z.W. Seh, Y. Sun, Q. Zhang, Y. Cui, Designing high-energy lithium-sulfur batteries, Chem. Soc. Rev. 45 (2016) 5605–5634, https://doi.org/10.1039/c5cs00410a.
[13] T. Cleaver, P. Kovacik, M. Marinescu, T. Zhang, G. Offer, Perspective—Commercializing Lithium Sulfur Batteries: Are We Doing the Right Research? J. Electrochem. Soc. 165 (2017) https://doi.org/10.1149/2.0071801jes.
[14] H. Lin, R. Jin, A. Wang, S. Zhu, H. Li, Transition metal embedded C2N with efficient polysulfide immobilization and catalytic oxidation for advanced lithium-sulfur batteries: a first principles study, Ceram. Int. 45 (2019) 17996–18002.
[15] R. Cao, W. Xu, D. Lv, J. Xiao, J.-G. Zhang, Anodes for Rechargeable Lithium-Sulfur Batteries, Adv. Energy Mater. 5 (2015) 1402273, https://doi.org/10.1002/aenm.201402273.
[16] X. Ji, K.T. Lee, L.F. Nazar, A highly ordered nanostructured carbon-sulphur cathode for lithium-sulphur batteries, Nat. Mater. 8 (2009) 500–506, https://doi.org/10.1038/nmat2460.
[17] J. Schuster, G. He, B. Mandlmeier, T. Yim, K.T. Lee, T. Bein, L.F. Nazar, Spherical ordered mesoporous carbon nanoparticles with high porosity for lithium-sulfur batteries, Angew. Chem. 51 (2012) 3591–3595, https://doi.org/10.1002/anie.201107817.
[18] J.-Q. Huang, X.-F. Liu, Q. Zhang, C.-M. Chen, M.-Q. Zhao, S.-M. Zhang, W. Zhu, W.-Z. Qian, F. Wei, Entrapment of sulfur in hierarchical porous graphene for lithium–sulfur batteries with high rate performance from− 40 to 60° C, Nano Energy 2 (2013) 314–321.
[19] Z. Liang, X. Fan, D.J. Singh, W. Zheng, Adsorption and diffusion of Li with S on pristine and defected graphene, PCCP 18 (2016) 31268–31276.
[20] M. Yu, R. Li, M. Wu, G. Shi, Graphene materials for lithium–sulfur batteries, Energy Storage Mater. 1 (2015) 51–73.
[21] X.G. Sun, X. Wang, R.T. Mayes, S. Dai, Lithium–sulfur batteries based on nitrogen-doped carbon and an ionic-liquid electrolyte, ChemSusChem 5 (2012) 2079–2085.
[22] Y. Qiu, W. Li, W. Zhao, G. Li, Y. Hou, M. Liu, L. Zhou, F. Ye, H. Li, Z. Wei, High-rate, ultralong cycle-life lithium/sulfur batteries enabled by nitrogen-doped graphene, Nano Lett. 14 (2014) 4821–4827.
[23] J.-J. Chen, R.-M. Yuan, J.-M. Feng, Q. Zhang, J.-X. Huang, G. Fu, M.-S. Zheng, B. Ren, Q.-F. Dong, Conductive Lewis base matrix to recover the missing link of Li2S8 during the sulfur redox cycle in Li–S battery, Chem. Mater. 27 (2015) 2048–2055.
[24] H.J. Peng, T.Z. Hou, Q. Zhang, J.Q. Huang, X.B. Cheng, M.Q. Guo, Z. Yuan, L.Y. He, F. Wei, Strongly coupled interfaces between a heterogeneous carbon host and a sulfur-containing guest for highly stable lithium-sulfur batteries: mechanistic insight into capacity degradation, Adv. Mater. Interfaces 1 (2014) 1400227.
[25] Z. Wang, Y. Dong, H. Li, Z. Zhao, H. Bin Wu, C. Hao, S. Liu, J. Qiu, X.W.D. Lou, Enhancing lithium–sulphur battery performance by strongly binding the discharge products on amino-functionalized reduced graphene oxide, Nat. Commun. 5 (2014) 1–8.
[26] C. Tang, Q. Zhang, M.Q. Zhao, J.Q. Huang, X.B. Cheng, G.L. Tian, H.J. Peng, F. Wei, Nitrogen-doped aligned carbon nanotube/graphene sandwiches: facile catalytic growth on bifunctional natural catalysts and their applications as scaffolds for high-rate lithium-sulfur batteries, Adv. Mater. 26 (2014) 6100–6105.
[27] Q. Pang, L.F. Nazar, Long-life and high-areal-capacity Li–S batteries enabled by a light-weight polar host with intrinsic polysulfide adsorption, ACS Nano 10 (2016) 4111–4118.
[28] C. Wang, K. Su, W. Wan, H. Guo, H. Zhou, J. Chen, X. Zhang, Y. Huang, High sulfur loading composite wrapped by 3D nitrogen-doped graphene as a cathode material for lithium–sulfur batteries, J. Mater. Chem. A 2 (2014) 5018–5023.
[29] L. Zhang, P. Liang, X.-L. Man, D. Wang, J. Huang, H.-B. Shu, Z.-G. Liu, L. Wang, Fe, N co-doped graphene as a multi-functional anchor material for lithium-sulfur battery, J. Phys. Chem. Solids 126 (2019) 280–286.
[30] Q.-W. Zeng, R.-M. Hu, Z.-B. Chen, J.-X. Shang, Single-atom Fe and N co-doped graphene for lithium-sulfur batteries: a density functional theory study, Mater. Res. Express 6 (2019), 095620.
[31] T. Zhang, Z. Chen, J. Zhao, Y. Ding, Metal-N4/graphene as an efficient anchoring material for lithium-sulfur batteries: A computational study, Diam. Relat. Mater. 90 (2018) 72–78.
[32] L. Zhang, P. Liang, H.B. Shu, X.L. Man, X.Q. Du, D.L. Chao, Z.G. Liu, Y.P. Sun, H. Z. Wan, H. Wang, Design rules of heteroatom-doped graphene to achieve high performance lithium–sulfur batteries: both strong anchoring and catalysing based on first principles calculation, J. Colloid Interface Sci. 529 (2018) 426–431.
[33] Z. Liang, D. Yang, P. Tang, C. Zhang, J. Jacas Biendicho, Y. Zhang, J. Llorca, X. Wang, J. Li, M. Heggen, Atomically dispersed Fe in a C2N based catalyst as a sulfur host for efficient lithium–sulfur batteries, Adv. Energy Mater. 11 (2021) 2003507.
[34] Z. Liu, L. Zhou, Q. Ge, R. Chen, M. Ni, W. Utetiwabo, X. Zhang, W. Yang, Atomic iron catalysis of polysulfide conversion in lithium–sulfur batteries, ACS Appl. Mater. Interfaces 10 (2018) 19311–19317.
[35] Y. Tao, Y. Wei, Y. Liu, J. Wang, W. Qiao, L. Ling, D. Long, Kinetically-enhanced polysulfide redox reactions by Nb 2 O 5 nanocrystals for high-rate lithium–sulfur battery, Energy Environ. Sci. 9 (2016) 3230–3239.
[36] G. Babu, N. Masurkar, H. Al Salem, L.M.R. Arava, Transition metal dichalcogenide atomic layers for lithium polysulfides electrocatalysis, J. Am. Chem. Soc. 139 (2017) 171–178.
[37] C. Zheng, S. Niu, W. Lv, G. Zhou, J. Li, S. Fan, Y. Deng, Z. Pan, B. Li, F. Kang, Propelling polysulfides transformation for high-rate and long-life lithium–sulfur batteries, Nano Energy 33 (2017) 306–312.
[38] C. He, Y. Liang, W. Zhang, Design of Novel Transition-Metal-Doped C6N2 with High-Efficiency Polysulfide Anchoring and Catalytic Performances toward Application in Lithium-Sulfur Batteries, ACS Appl. Mater. Interfaces 14 (2022) 29120–29130.
[39] J. Kim, S.J. Kim, E. Jung, D.H. Mok, V.K. Paidi, J. Lee, H.S. Lee, Y. Jeoun, W. Ko, H. Shin, Atomic Structure Modification of Fe-N-C Catalysts via Morphology Engineering of Graphene for Enhanced Conversion Kinetics of Lithium-Sulfur Batteries, Adv. Funct. Mater. 2110857 (2022).
[40] A, G.K.; b, J.F. Efficiency of ab-initio total energy calculations for metals and semiconductors using a plane-wave basis set - ScienceDirect. Comput. Mater. Sci., 1996, 6, 15–50.
[41] G.G. Kresse, J.J. Furthmüller, Efficient Iterative Schemes for Ab Initio Total-Energy Calculations Using a Plane-Wave Basis Set, Phys. Rev. B: Condens. Matter 54 (1996) 11169.
[42] G. Kresse, D. Joubert, From ultrasoft pseudopotentials to the projector augmented-wave method, Physical Review B 59 (1999) 1758–1775.
[43] J.P. Perdew, K. Burke, M. Ernzerhof, Generalized Gradient Approximation Made Simple, Phys. Rev. Lett. 77 (1998) 3865–3868.
[44] H.J. Monkhorst, J.D. Pack, Special points for Brillouin-zone integrations, Phys. Rev. B (1976).
[45] S.P. Jand, Y. Chen, P. Kaghazchi, Comparative theoretical study of adsorption of lithium polysulfides (Li2Sx) on pristine and defective graphene, J. Power Sources 308 (2016) 166–171.
[46] H. Sun, M. Wang, X. Du, Y. Jiao, S. Liu, T. Qian, Y. Yan, C. Liu, M. Liao, Q. Zhang, Modulating the d-band center of boron doped single-atom sites to boost the oxygen reduction reaction, J. Mater. Chem. A 7 (2019) 20952–20957.
[47] S. Lu, H.L. Huynh, F. Lou, K. Guo, Z. Yu, Single transition metal atom embedded antimonene monolayers as efficient trifunctional electrocatalysts for the HER, OER and ORR: a density functional theory study, Nanoscale 13 (2021) 12885–12895.